Block Copolymer Nanocontainers

Marco Pinna,[†,*] Stephanie Hiltl,[‡] Xiaohu Guo,[†,§] Alexander Böker,[‡,*] and Andrei V. Zvelindovsky[†,*]

[†]Computational Physics Group, University of Central Lancashire, Preston PR1 2HE, United Kingdom, and [‡]DWI an der RWTH Aachen e.V., Lehrstuhl für Makromolekulare Materialien und Oberflächen, RWTH Aachen University, D-52056 Aachen, Germany. [§]Present address: Computational Science & Engineering Department, Daresbury Laboratory, Warrington, WA4 4AD, United Kingdom.

ARTICLE

ABSTRACT Using cell dynamics computer simulation, we perform a systematic study of thin block copolymer films around a nanoparticle. Lamellar-, cylinder-, and sphere-forming block copolymers are investigated with respect to different film thicknesses, particle radii, and boundary conditions at the film interfaces. The obtained structures include standing lamellae and cylinders, "onions", cylinder "knitting balls", "golf ball", layered spherical, "virus"-like and mixed morphologies with T-junctions and U-type defects. The kinetics of the structure formation and difference with planar thin films are discussed. Our simulations suggest that novel porous nanocontainers can be formed by the coating of a sacrificial nanobead by a block copolymer layer with a well-controlled nanostructure. In addition, first scanning force microscopy experiments on a model system reveal surface structures similar to those predicted by our simulations.

KEYWORDS: block copolymer · computer simulation · spherical particle · scanning force microscopy · nanocapsule

Block copolymers (BCPs) are molecules composed of different blocks covalently connected into one macromolecule. They can assemble into a variety of ordered structures with intradomain distances in the range of 10−100 nm. Classical structures in bulk are lamellae, hexagonally ordered cylinders, body-centered cubic arrays of spheres and more complex structures like the gyroid. These structures are of great interest and importance due to possible applications in nanotechnology, as for example the use of block copolymer films as masks for nanolithography, fabrication of nanoporous membranes for advanced separation media and photonic crystals.[1−4] In addition, block copolymers can serve as building material for intelligent nanosize bioreactors and vesicles as drug delivery vehicles or self-regulating diagnostic devices.[5,6] The problem of using BCPs lies in the control of their nanostructure. There is a large number of experimental and theoretical works which address the problem of tailoring a desired nanostructure.[1] Applied external fields are promising candidates to achieve that goal. Such fields can be surface fields,[7−13] electric field,[7,14−20] and shear flow.[7,16,17,21] Surface fields are, in particular, prominent in confined geometries. Confinement is a powerful tool in breaking the symmetry of a structure, allowing materials to self-assemble into new morphologies that usually are not present in the bulk. Symmetric and asymmetric block copolymers have been studied in thin film confinement both experimentally[10,11,13,14,22,23] and theoretically.[13,24−28] However, the confinement in a thin film is essentially one-dimensional (1D) confinement. Depending on the attraction of one type of block to the surface (surface field) and the natural microdomain spacing of a system, which normally forms cylinders in the bulk, one can observe structures like perforated lamellae, parallel or perpendicular (with respect to the surface) lamellae or cylinders.[29−31] There have been very recent works on block copolymer self-assembly in cylindrical nanopores, both experimental[32−35] and computational.[24,36−47] In the case of the cylindrical pore geometry, in addition to surface field and commensurability, the curvature influences the morphology. The curvature effect is the subject of growing interest in the literature.[48,49] Due to restrictions in two directions, the confinement in a cylindrical pore is essentially a two-dimensional (2D) confinement. It leads to the formation of new structures not found in bulk or in planar films. The spherical confinement differs from that in a cylinder where one of the principal curvatures is zero; this is a three-dimensional (3D) confinement. Very recently, the spherical confinement has attracted extensive attention of the scientific community. There are many

*Address correspondence to mpinna@uclan.ac.uk, boeker@dwi.rwth-aachen.de, avzvelindovsky@uclan.ac.uk.

Received for review April 28, 2009 and accepted April 21, 2010.

Published online May 25, 2010. 10.1021/nn901853e

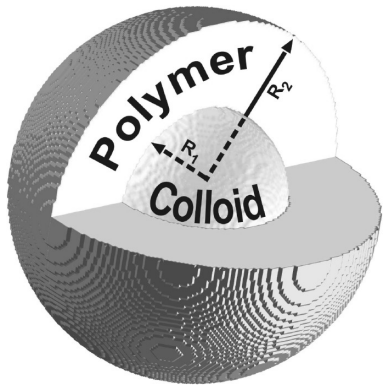

Figure 1. Schematic representation of the proposed system.

experimental works trying to create particles with various inner structures.[50−58] Tajima *et al.* found hemispherical and core−shell particles which consist of a mixture of two homopolymers.[56] The structure of these particles can be controlled by changing the concentration of the polymer solution. Higuchi *et al.* prepared block copolymer nanostructured particles with lamellar, onion-like, and hexagonally packed cylindrical structure depending on the block ratio and the concentration of solution.[55,58] Rider *et al.* studied the 3D confinement of lamellae and cylinder-forming BCPs in silica colloidal and inverse colloidal crystals. They found a variety of structures such as nontrivially packed BCP spheres, lamellar onions, and more complex "golf-ball"-type morphology.[57] Previous computer simulations focused on BCPs confined on a surface of a sphere in 2D, which is an idealized model of infinitely thin BCP films[59,60] or on modeling of BCP vesicles[61,62] and BCP droplets.[36,63,64] In an experimentally realistic situation, BCP film morphologies will strongly depend on the film thickness,[30] and therefore, many film morphologies cannot be reduced to patterns on the infinitely thin 2D spherical surface. It was suggested in ref 60 that a full 3D treatment is necessary in order to enable the design of functional colloids and nanoparticles with copolymers adsorbed, coated, or grafted on their surfaces.

Here, we study systems schematically shown in Figure 1, where a BCP film covers a nanoparticle of radius R_1. The film is confined between two spherical interfaces with radii R_2 and R_1, which is essentially different from the case of BCP droplets where $R_1 = 0$. If the colloid is chemically removed after the BCP film is formed, a nanoshell structure can be obtained and serve as nanocontainer for various applications mentioned above. In our previous short communication, we reported on one limiting case of such systems where both interfaces have the same affinity to the copolymer block and only for a couple of film thicknesses.[65] In general, both interfaces (with the internal nanoparticle and with the surrounding environment) can have very different surface energies with respect to BCP. Here, we perform a systematic study of spherically curved BCP films varying all relevant parameters: interaction of inner and outer surfaces with BCP blocks, film thickness, as well as BCP composition. Our simulations nicely match first experimental results on a model system with a half-sphere substrate geometry, where a thin film of a cylinder-forming BCP has been floated onto a surface constructed from silica nanoparticles sintered onto a silicon oxide surface.

RESULTS AND DISCUSSION

In the present work, we study AB diblock copolymers in the geometry depicted in Figure 1. The inner spherical surface with radius R_1 represents the surface of the nanoparticle. The outer surface with radius R_2 models the interface between the diblock copolymer film and the surrounding medium. Therefore, the film thickness is $d = R_2 - R_1$.

Lamellae-Forming System. For a lamellae-forming system, we chose the simplest case of symmetric diblock copolymer with equal volume fractions of both blocks, $f = 0.5$. The other parameters entering in eq 2 are $D = 0.5$, $B = 0.02$, $\tau = 0.36$, $u = 0.5$ (this parameter can be expressed in terms of the Flory−Huggins parameter, the degree of polymerization, and the monomer size; see eq 4). We consider two cases: one where both surfaces have the same preference to a given copolymer block, and another when the affinity to the copolymer block is different at each surface. In describing our results, we use a characteristic length scale L_0, which is the domain spacing in the bulk lamellae. In our simulation, it is measured to be $L_0 \approx 8$ grid points.

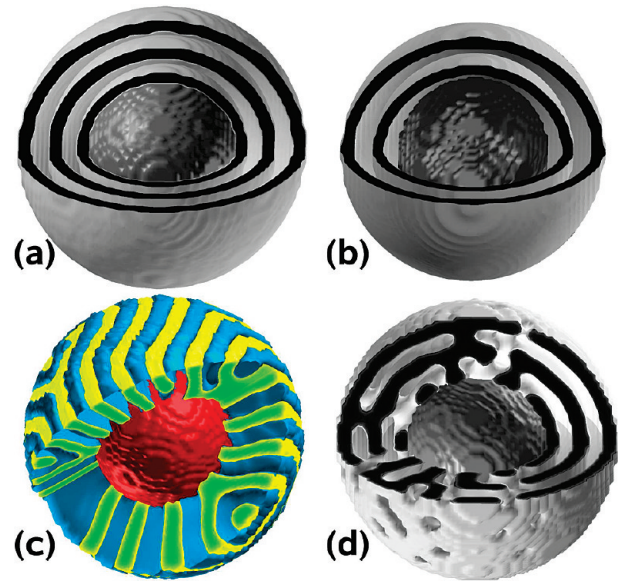

Figure 2. Symmetric lamellae shells which are cut in 1/4 to show the particle inside. $R_1 = 16$ and $R_2 = 32$ grid points ($d/L_0 = 2$). The boundary conditions $\psi_1 = \psi_2 = \psi_0$ are: (a) 0.4, (b) −0.4, (c) 0, (d) 0.2.

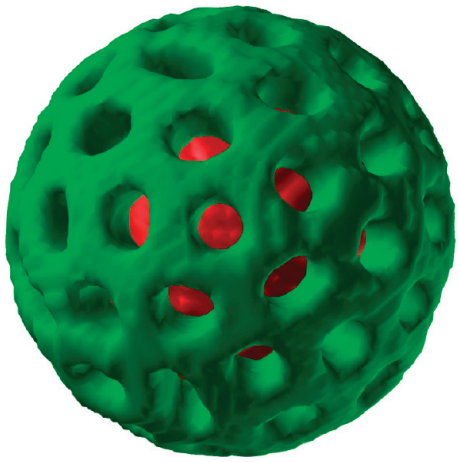

Figure 3. Golf-ball morphology. $R_1 = 16$ and $R_2 = 22$ grid points ($d/L_0 = 0.75$). The boundary conditions are $\psi_0 = 0.2$.

Similar Interfaces. First, we consider similar interfaces $\psi_1 = \psi_2 = \psi_0$. This is the same situation as in ref 65. However, in addition to our earlier results, we study a much wider range of parameters which helped to discover additional new morphologies and explain formation of golf-ball morphology. Moreover, here we present dynamics of the morphologies, while ref 65 presents only static results. Figure 2 shows the results for lamellae morphologies for various surfaces conditions. The value ψ_0 at the boundary describes the preference of one block to the surface.

Preferable affinity of one of the blocks to the surface induces lamellae being wrapped around a nanoparticle (Figure 2a). Changing the surface preference to another block, we can flip the lamellae sequence (say, AB to BA; Figure 2b). The morphology is similar to parallel lamellae $L_\parallel$ in the planar thin films.[12] Similar onion-like structures have been seen by transmission electron microscopy in ref 57 (Figure 7 therein) as well as in ref 58 (Figure 1 therein). In the case of neutral surfaces, $\psi_0 = 0$, the lamellae stand up as shown in Figure 2c. The situation is similar but not identical to perpendicular lamellae $L_\perp$ in planar thin films.[12] In a spherical geometry, the curvature changes with the radius. Therefore, purely perpendicular lamellae cannot exist as they cannot be always parallel to each other. We observe two types of defects which are necessary to allow the $L_\perp$ morphology to adapt itself to the spherical geometry. As a result, either standing lamellae become thicker when the radius increases or they develop characteristic Y-shape defects (Figure 2c). Both situations do not occur in planar thin films. Such a structure is yet to be found in experiments. However, the results in ref 57 (Figure 4 therein), where standing lamellae are found between densely packed colloids, are an indirect confirmation that structures similar to those shown in Figure 2c can exist. For an intermediate strength of the surface interaction, a mixed morphology develops combining both $L_\parallel$ and $L_\perp$ (Figure 2d), as both $L_\parallel$ and $L_\perp$ orientations compete with each other near the surface. This mixed lamellar morphology requires many defects in the form of perforations and channels (Figure 2d). In confined systems, not only surface affinity but also the ratio between L_0 and d is important. For instance, if a mismatch exists between L_0 and d, it can lead to extensional forces that may stabilize structures normally not stable in the bulk. This situation is demonstrated in Figure 3, where a single perforated lamellae (PL) sheet develops. This is similar to the situation in the planar thin films.[29] However, the PL morphology wrapped around a sphere does not always show a hexagonal arrangement of perforations, but a mixture of 5 and 6 neighboring perforations (Figure 3). Recently, Rider *et al.* reported such morphology as golf-ball morphology for a diblock copolymer system in silica colloidal crystals.[57] In general, the structure is rather sensitive to the degree of confinement. For instance, different morphologies are shown in Figure 4 for different thicknesses (different ratio d/L_0). With increasing shell thickness, the morphology gradually changes from one lamellar sheet to two lamellae. When the film thickness is small, the lamella is thinner compared to thicker films (see Figure 4a,b). The intermediate structure is a PL where initially very few perforations form (see Figure 4b). Their number increases with the increasing of film thickness, until the compact packing of perforations is reached (see Figure 4c,d). A similar situation can be seen for larger sphere radii (Figure 5). An interesting observation is that the perforated lamellae morphology is not symmetric with respect to the inner and outer surfaces. While it is smooth at the outer surface (Figure 5a), it forms labyrinth-like structure at the inner surface (Figure 5b). In fact, this structure is a hybrid morphology. Hybrid morphologies are found in thin planar films with asymmetric boundary conditions.[27] Although our surfaces are symmetric here, the symmetry breaking occurs due to the different curvatures of both surfaces. In-

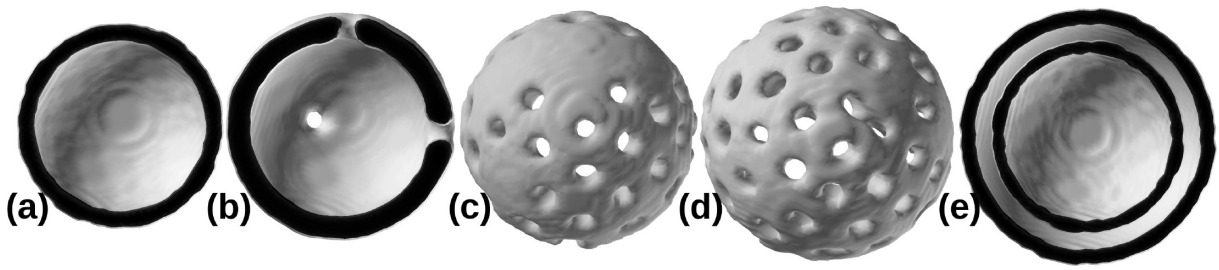

Figure 4. Evolution of lamellar structure with $\psi_0 = 0.4$ and $R_1 = 16$ for different values of thickness d (d/L_0): (a) 4 (0.5), (b) 6 (0.75), (c) 7 (0.875), (d) 8 (1), (e) 9 (1.125). For a better view, we show only half shells.

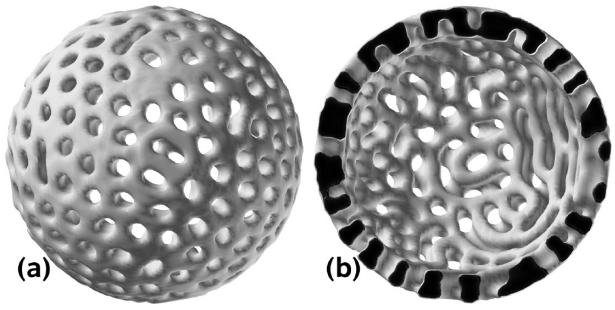

Figure 5. PL morphology with $R_1 = 32$ and $R_2 = 40$, $\psi_0 = 0.4$.

ner and outer layers have different structures. In fact, these are two different morphologies (perforated and standing lamellae) merged in a hybrid morphology. Structures in inner and outer layers do not always correspond to each other. For instance, an elongated perforation in the outer layer can meet a neck-bridge in the inner layer (see Figure 5a) and *vice versa*: an indentation of the inner layer sometimes does not reach the outer surface forming Π-type arches seen in Figure 5b.

The PL structure can be obtained in different ways, for instance, by varying the surface interaction (see Figure 3) or the film thickness (see Figure 4b).Figure 6 shows two different pathways of the PL structure formation. The top row of Figure 6 shows the transformation of an initially equilibrated structure when the surface interaction was changed from $\psi_0 = 0.4$ to $\psi_0 = 0.2$. The bottom row of Figure 6 shows the development of the structure starting from a different initial condition, namely, from a disordered state. The visual inspection alone is not sufficient to describe all details of the morphological pathways. Therefore, both evolution pathways have been analyzed using the Minkowski functionals that give a quantitative picture of the morphological transitions. In 3D, there are four Minkowski functionals: volume (V), surface area (S), mean curvature ($2H$), and Euler number (χ).[16,73,74] The Euler number is directly related to the integral Gaussian curvature and is a measure of the topology of the structure.

The left picture in the top row of Figure 6 is obtained after 500 000 time steps of equilibration with $\psi_0 = 0.4$. The morphology consists mostly of single lamellar sheets with a few non-ordered perforations. At the beginning of the simulation, we change the value of ψ_0 to 0.2, which results in an increase in volume at the first instant. This increase can be attributed to the fact that the change of the boundary condition from $\psi_0 = 0.4$ to 0.2 partially relaxes the "squeezing" of the lamella which becomes slightly thicker. At the later stages, the volume decreases as a result of many perforations forming in the lamellar sheet. The surface area increases monotonically during the whole process as holes and undulations (see second picture in the top row of Figure 6) increase the surface. The behavior of the mean curvature is less trivial: it stays almost constant until 500 time steps in spite of many undulations in the lamellar surface (see second picture in the top row of Figure 6). The increase of the mean curvature by these undulations is counter balanced by the increasing perforation radii (compare the first two images in the top row of Figure 6), which reduces the mean curvature. As soon as new perforations appear, the mean

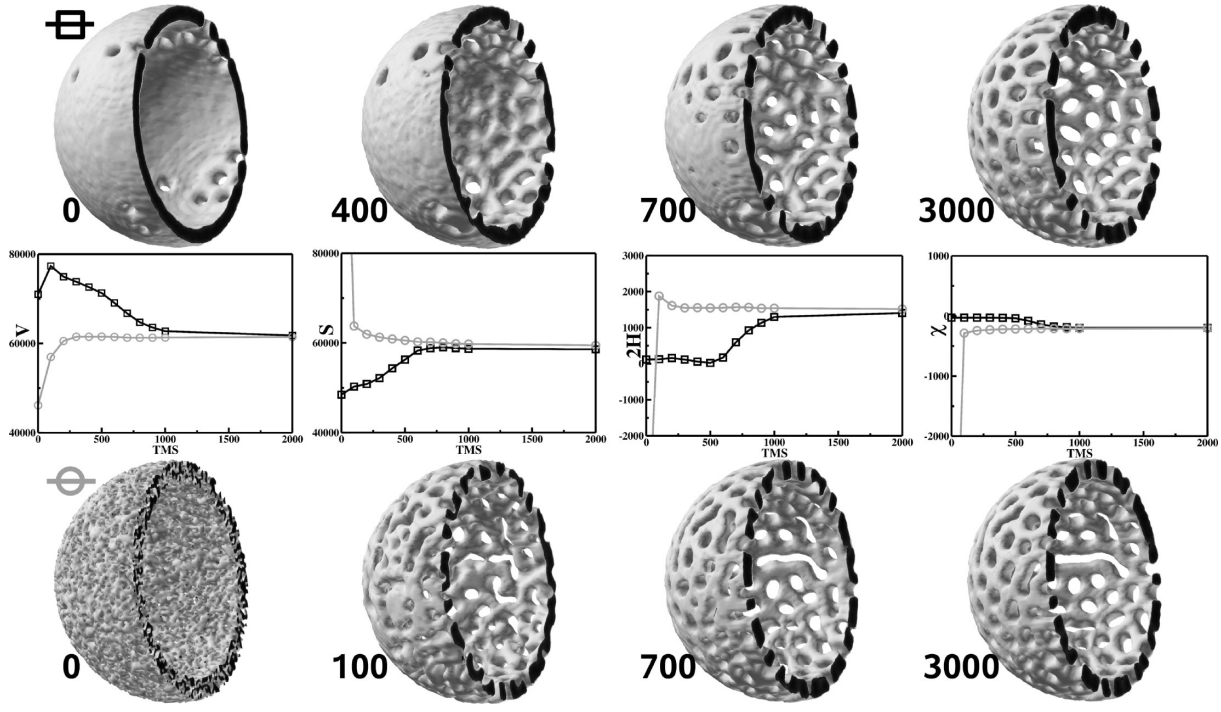

Figure 6. Kinetic pathway of PL morphology formation. $R_1 = 32$, $R_2 = 38$ with noise $\eta = 0.02$. Top (□): Evolution starting from the morphology with $\psi_1 = \psi_2 = \psi_0 = 0.4$ after an equilibration for 500 000 time steps (0 time step) and changing ψ_0 to 0.2. Bottom (○): Evolution starting from a disordered state (0 time step) for $\psi_1 = \psi_2 = \psi_0 = 0.2$. In the middle: Minkowski functionals as a function of time step (TMS): (V) volume, (S) surface, ($2H$) curvature, (χ) Euler number.

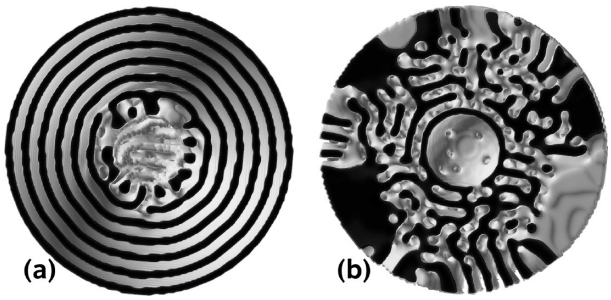

Figure 7. Hybrid systems, $R_1 = 16$ and $R_2 = 64$ and ratio $d/L_0 = 6$: (a) $\psi_1 = 0$ and $\psi_2 = 0.4$; (b) $\psi_1 = 0.4$ and $\psi_2 = 0$.

curvature starts to increase (see the third images in the top row). That behavior can be confirmed from the Euler characteristic plot, which shows χ being constant until about 500 time steps and decreasing after that (χ decreases because every hole is equivalent to -1). The kinetic pathway of the second system is different, but the final structure is the same. The starting configuration is a disordered state (see the left image in the bottom row). A microphase separation proceeds as the volume increases, while the surface area decreases as the structure coarsens (initial small micelles merge and increase in size). As a result of coarsening, the mean curvature decreases and the Euler characteristic increases (less holes). An important observation is that the second system is faster than the first one. It indicates that it is easier to form a PL morphology starting from a disordered state than from a previously equilibrated lamellar morphology.

Dissimilar Interfaces. In the previous subsection, we studied diblock copolymer films confined between two concentric spherical surfaces which have the same affinity to the copolymer blocks. In this subsection, we investigate the morphologies when the two surfaces have a different affinity to the blocks. Such a situation is more realistic as the affinity of the surrounding environment and the surface of the nanoparticle to the copolymer is different, especially if solvents are present in the surrounding media. In such a case, we can obtain a hybrid structure as a mixed morphology between $L_\parallel$ and $L_\perp$ (see Figure 7). Hybrid structures are also found in planar thin films;[27] however, the extent of the surface influence is different in planar and spherical geometries. Figure 7 shows two different cases: (a) when the outer surface prefers one of the blocks while the inner surface is neutral, and (b) *vice versa*. A preferential surface induces $L_\parallel$, while neutral surface induces $L_\perp$. The outer surface has always the largest influence on the morphology due to its large surface area. Parallel lamellae in Figure 7a propagate inside the film for several layers, while $L_\perp$ extends from the inner surface only for the distance of only one domain spacing distance. When both morphologies meet inside the film, they form T-junctions (see Figure 7). In addition "the meeting point" ($L_\perp L_\parallel$ hybrid) has many perforations. A similar situation occurs in Figure 7b, but $L_\perp L_\parallel$ switch their places: $L_\perp$ propagates from the outer neutral surface far within the film, while $L_\parallel$ extends only for one layer around the inner particle. This layer has perforations, however, without dense packing. There are only occasional patches of $L_\parallel$ inside the film. When $L_\parallel$ and $L_\perp$ meet, they form T-junctions. The inner structure of the film is rather defected, which is attributed to the fact that when $L_\perp$ lamellae propagate inside the film their intralamellar distance has to change with radius and defects necessarily form. By varying the interaction of blocks with both surfaces and the film thickness, we can induce more exotic structures like a "virus morphology" in Figure 8. This morphology is, in fact, an asymmetric PL morphology. Instead of showing the perforated component, we show the matrix component which consists of an inner leaf surrounding the nanoparticle, with cylindrical necks. The outer leaf, which is normally present in a symmetric PL (Figure 3), does not develop due to the asymmetric boundary conditions of Figure 8.

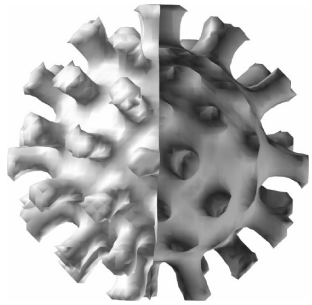

Figure 8. Virus structure for $\psi_1 = 0.4$ and $\psi_2 = 0.2$; $R_1 = 16$ and $R_2 = 22$. Shell is cut in 1/4.

Cylinder-Forming System. In this section, we consider cylindrical morphology with $f = 0.4$. The other parameters are $D = 0.5$, $B = 0.02$, $\tau = 0.30$, $u = 0.5$, and $v = 1.5$. All simulations were carried out for 500 000 time steps. The distance between cylinders in the bulk is found to be $L_0 \approx 8$ grid points.

Similar Interfaces. Figure 9 shows a cylinder-forming system between surfaces which have the same affinity to the copolymer blocks. In the case of cylinders, the situation is similar to the case of the lamellar morphology. Selective surfaces induce the formation of parallel cylinders ($C_\parallel$, see Figure 9a), while between the neutral or slightly selective surfaces, perpendicular cylinders ($C_\perp$, see Figure 9d) form. In order to verify these results, we performed scanning force microscopy experiments on thin BCP films floated onto half-spheres on a silicon wafer (see Figure 9b,e). In order to obtain the equilibrium structures, the films were annealed either in solvent vapor or above the glass transition temperature. Here, we switched from a selective surface such as silicon oxide to a less selective one by addition of a carbon coating. Figure 9e,f shows the topography and phase image of a 40 nm thick BCP film on a carbon-coated sphere of 520 nm diameter. The cylinder domain spacing is about 32 nm. Clearly, perpendicular cylinders can be seen as bright spots in the phase image (Figure 9f). The halo on the right-hand side of the spheres in the

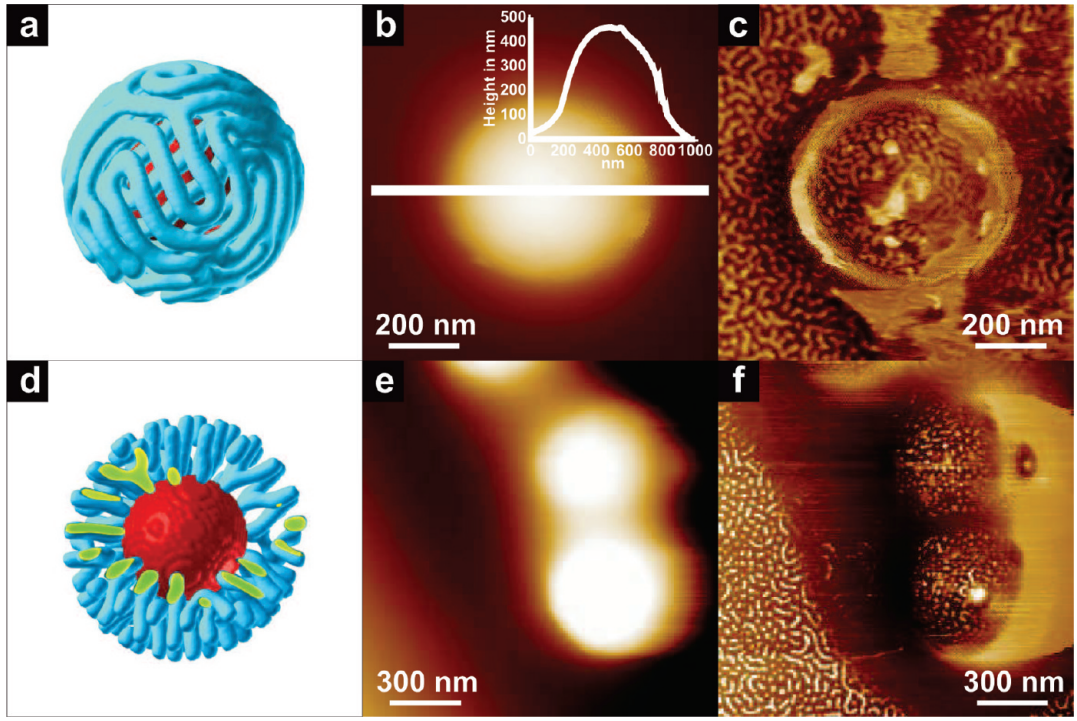

Figure 9. Nanoshells from cylinders. (a,d) Simulations. $R_1 = 16$ and $R_2 = 32$ grid points and ratio $d/L_0 = 2$. The boundary conditions ψ_0 are (a) 0.4, (d) −0.1. (b,c,e,f) SFM images of 40 nm PS-*b*-PB film on 520 nm diameter silica spheres. (b) Topography and (c) phase image of BCP on pure silicon oxide surface with preference for PB. (e) Topography image and (f) phase image of the same film on a carbon-coated surface (neutral toward PS and PB). The inset in (b) shows a cross section along the line indicated.

phase image is an artifact originating from the steep height difference between particle and the flat surface. In the case of a pure silicon oxide surface, the phase image reveals cylinders predominantly aligned parallel to the particle surface (Figure 9c). Figure 9a shows that in order to wrap several layers around a sphere the neighboring layers lay mostly perpendicular to each other. The two layers of $C_{\parallel}$ in Figure 9a are obtained for the ratio $d/L_0 = 2$. A layer of $C_{\parallel}$ can be formed, decreasing the shell thickness (Figure 10). Similar morphologies, $C_{\parallel}$ and $C_{\perp}$, have been obtained in thin planar films, as well.[26,27] However, in planar films, the standing up cylinders can form hexagonal arrays of cylinders that are not possible in the spherical geometry due to the curvature (Figure 9f). Standing cylinders have defects in order to accommodate the curvature around the spherical nanoparticle. They are Y-shaped defects and dislocations when a shorter cylinder squeezes between longer ones (Figure 9d). Sometimes, short perpendicular cylinders are identical to spheres. This can be interpreted as a shift in the phase diagram into the coexistence of cylinders and spheres. Another shift can be obtained by changing the shell thickness (Figure 10). When the ratio d/L_0 is equal to 0.75, the structure con-

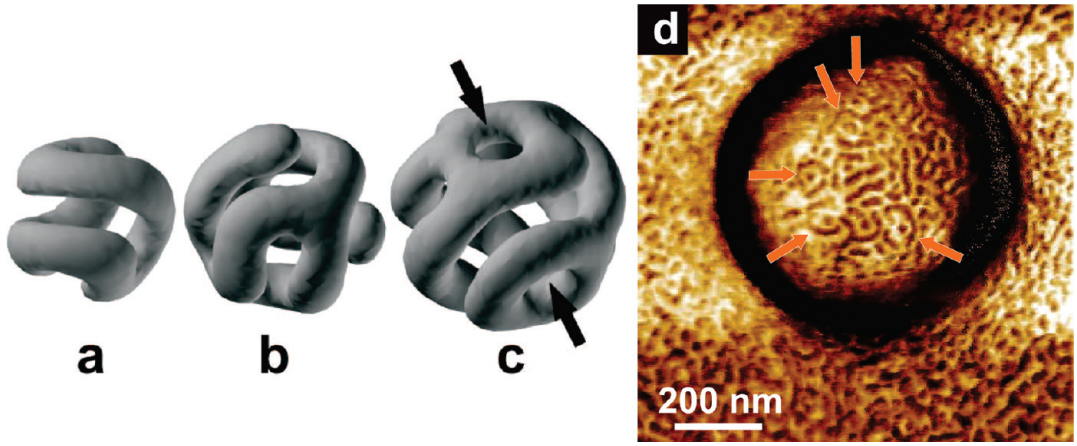

Figure 10. (a−c) Simulation of cylinder shells with ψ_0 =0.4 and $R_1 = 4$ for different thicknesses $R_2(d/L_0)$: (a) 10 (0.75), (b) 12 (1), (c) 14 (1.25). (d) SFM phase image of a BCP film on a sphere at a ratio (d/L_0) of 1.25 after extensive annealing. The arrows in (c) and (d) point to characteristic perforations.

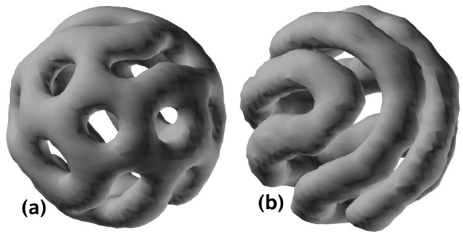

Figure 11. Shell with $R_1 = 8$, $R_2 = 16$ and $\psi_0 = 0.4$ for different noise value η: (a) 0, (b) 0.02.

sists of only one curved cylinder without defects (see Figure 10a). When the ratio of d/L_0 was increased, the cylinders become interconnected (see Figure 10b) until a perforation forms like in the PL case (see Figure 10c). Thus, a coexistence of different phases can be found. Horvat *et al.* found theoretically a coexistence of $C_\parallel$ and PL depending on the surface interaction and on the film thickness in a planar geometry[26] (see also experimental works in refs 30 and 31). In our SFM experiments, we could also verify such a coexistence for a thin BCP film on a silica sphere after extended annealing (Figure 10d). The image shows a BCP film at exactly the same ratio (d/L_0) of 1.25 as simulated in Figure 10c. Interestingly, we find perforations very similar to the ones existing in the simulations. The coexistence of the two phases ($C_\parallel$ and PL) can be also obtained for a larger nanoparticle (Figure 11a). It can be demonstrated that PL phase is a transient kinetically trapped phase: after application of the noise at every time step, only cylinders survive (Figure 11b).

Dissimilar Interfaces. In the section on lamellae, we present that different interactions between the two surfaces and the diblock copolymer can induce new morphologies. Lyakhova *et al.* studied theoretically the effect of dissimilar interfaces in thin planar films for cylinder-forming block copolymers and found different hybrid structures. Here, we study the two confining surfaces that favor cylinders of different orientation ($C_\perp$, $C_\parallel$). The top half of Figure 12 shows the results when the outer surface favors $C_\perp$, while the inner one favors $C_\parallel$. In the bottom half of Figure 12, the preferential orientation at surfaces is opposite. In Figure 12a (top), the ratio d/L_0 is 0.75, which is less than the typical domain spacing for cylinders in the bulk. We observe the shift toward the spherical phase (S) where all "spheres" are slightly flattened and asymmetric in shape due to the dissimilar interfaces. When $d = 8$ ($d/L_0 = 1$, in Figure 12b, top), the spheres become a bit more elongated (short $C_\perp$). These cylinders are slightly asymmetric in shape (compare with shape modulations in thin films, Figure 8a in ref 27). The fact that all cylinders are standing is due to a more pronounced influence of a larger surface (outer surface), which prefers $C_\perp$. A stronger influence of the outer surface was also seen in the case of the lamellar system in the previous section. When the shell is thicker, $d = 10$ ($d/L_0 = 1.25$) and $d = 12$ ($d/L_0 = 1.5$) in Figure 12c,d (top), we observe coexistence between $C_\parallel$ and $C_\perp$ as well as formation of U-like hybrids.

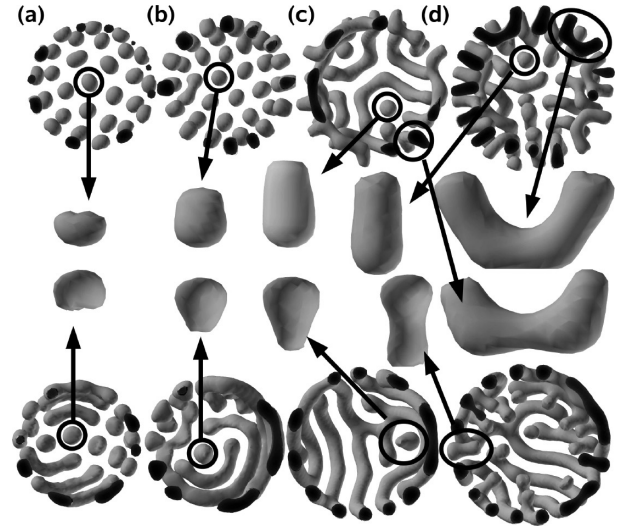

Figure 12. Hybrid structures for $R_1 = 16$ and different R_2: (a) 22, (b) 24, (c) 26, (d) 28. Top pictures have $\psi_1 = 0.4$ and $\psi_2 = -0.1$, while the bottom pictures have $\psi_1 = -0.1$ and $\psi_2 = 0.4$.

Similar hybrid has been seen in planar thin films (Figure 7 in ref 27). However, the angle between the arms of the U-hybrid is larger for a spherical confinement, and the thicker the film is the longer they are. When the boundary conditions are inverted, $\psi_2 = 0.4$ and $\psi_1 = -0.1$ (Figure 12, bottom), the results are different. Figure 12a (bottom) ($d/L0 = 0.75$) shows a coexistence of short modulated $C_\parallel$ with some necks and squeezed spheres. Modulated $C_\parallel$ are similar to ones found in planar thin films in Figure 8b of ref 27. The spheres are asymmetric in shape similar to the ones in Figure 12a (top), but with the opposite orientation. The dominant presence of $C_\parallel$ is due to the effect of the outer surface, which prefers this morphology. For thicker films ($d/L_0 = 1$ and $d/L_0 = 1.25$), the fraction of $C_\parallel$ becomes larger and squeezed spheres are replaced by $C_\perp$. Standing cylinders have a conical shape, which is enhanced by the spherical curvature (in the case of planar films, only very mild conical shapes have been ob-

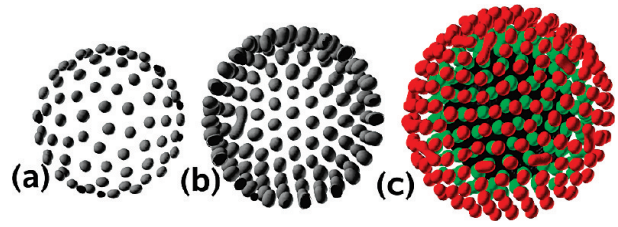

Figure 13. Spherical shells with $R_1 = 32$ and $\psi_0 = 0.4$ and different R_2: (a) 40, (b) 48, (c) 56.

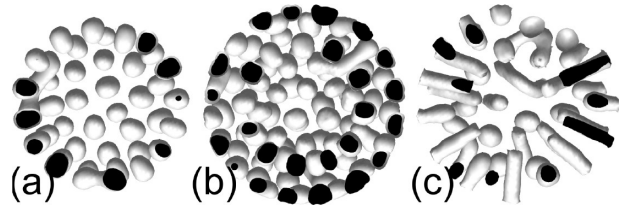

Figure 14. Induced transition between spherical and hybrid shells: $R_1 = 16$, $R_2 = 32$; $\psi_0 =$ (a) 0.4, (b) 0, (c) −0.3.

served as seen in Figure 8a in ref 27). When d = 12 (Figure 12d, bottom), we observe a coexistence of $C_{\parallel}$ with necks and $C_{\perp}$. The necks always point inward as the inner surface favors $C_{\perp}$. The remaining standing cylinders have dumbbell shape (Figure 12b, bottom, and Figure 9 in ref 27). Sometimes instead of $C_{\parallel}$ with necks, an external layer of $C_{\parallel}$ and the internal layer of spheres are present (Figure 12d; see also Figure 7 in ref 27).

Sphere-Forming System. In this section, we consider spherical morphology with f = 0.4. The other parameters are D = 0.5, B = 0.01, τ = 0.20, u = 0.38, and v = 2.3. All simulations were carried out for 500 000 time steps. The distance between spheres in the bulk is found to be $L_0 \approx 11$ grid points.

For a d = 8, we obtain a very thin layer of squeezed spheres (see Figure 13a). These spheres have liquid-like ordering (many defects). When d = 16 (d/L_0 = 1.45), we obtain a layer of spheres with the classical ordering as pairs of 5 and 6 neighbors due to the spherical curvature. When d = 24 (d/L_0 = 2.18), we have two layers of spheres. In the Figure 13c, the first layer is depicted in red and the second one in green. The spheres in one layer are shifted with respect to the spheres in another layer (it is seen in the center of Figure 13c that a red sphere is surrounded by three green spheres). Figure 14 shows the effect of different values of the surface affinity on the diblock copolymer morphology. When the surfaces prefer the majority component, the result is identical to Figure 13b (although the curvature is quite different) with one layer of spheres and a couple of laying cylinders as a result of spheres merger. For the neutral walls, we obtained two layers of spheres for the same film thickness (see Figure 14b). When the surfaces favor the minority component of the diblock copolymer, the system shifts toward coexistence of $C_{\perp}$ and spheres (Figure 14b).

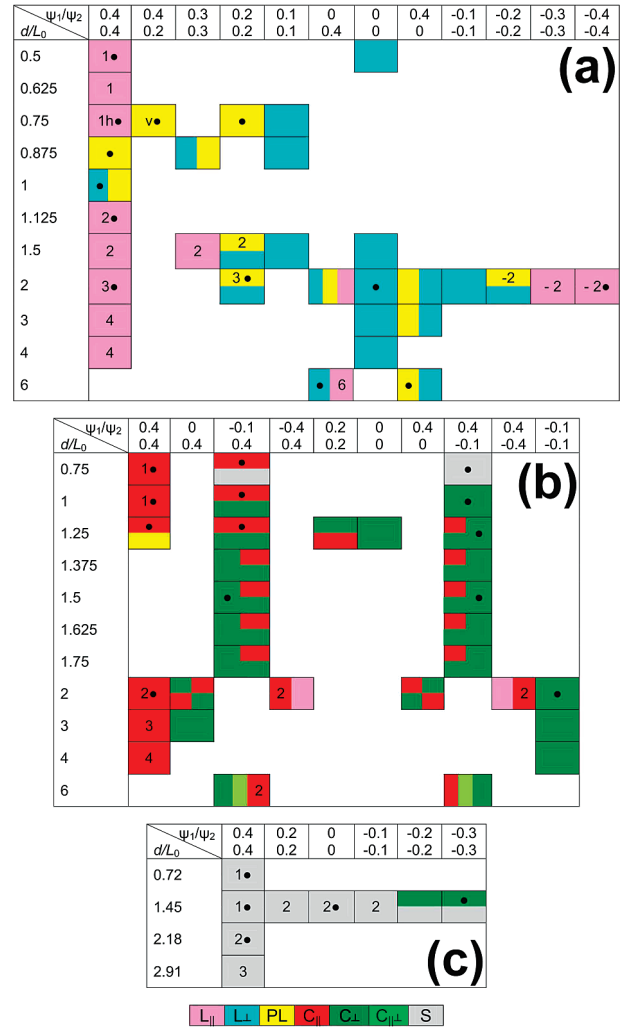

Figure 15. Nanoshell phase diagrams for different affinity of blocks to surfaces R_1 and R_2 and the film thickness d: (a) lamellar-forming system, (b) cylinder-forming system, (c) sphere-forming system. Each box represents a simulation result. The color code is given in a separate bar. Numbers represent the number of layers. Letters h and v are holes and virus, correspondingly. The minus sign indicates the inverse sequence of lamellae. The symbol $C_{\parallel\perp}$ is for mixed cylinders. For the structures with different morphologies in different layers, the boxes are split vertically, with the internal layers starting from the left. Horizontally split boxes indicate that morphologies coexist in the whole film or in a single layer with the top sub-box indicating the predominant morphology. Boxes with circles correspond to the structures shown in the paper.

SUMMARY

With the help of cell dynamics simulations, we investigated the morphologies of thin block copolymer films around a spherical nanoparticle and showed first experimental evidence for similar structures on model substrates. If after the preparation the film would be chemically cross-linked and the particle chemically removed, one would obtain nanoshells with the structure being controlled by the interplay between film thickness, block copolymer characteristics, surface parameters, as well as curvature. We found that we can control the structures ranging from standing lamellae or cylinders to lamellar "onions" and cylinder "knitting balls", hybrid structures with T-junction and U-type defects, layered spheres, and even more complex "golf-ball" and "virus" shells. Various structures are summarized in Figure 15. Such nanoshells can potentially serve as drug delivery vehicles and nanoreactors. CDS can be employed in the computer-aided design of such nanoshells.

METHODS

Computational. We employ a Ginzburg−Landau approach in the form of the cell dynamics simulation (CDS), which is a very fast computational technique[16,17,65−69,72] and can serve as a research precursor for more elaborate but slow methods. For an AB diblock copolymer, the structure can be described by an order parameter $\psi(\mathbf{r}, t) = \phi_A - \phi_B + (1 - 2f)$, where ϕ_A and ϕ_B are the local volume fractions of A and B monomers, respectively,

and f is the volume fraction of A monomers in the diblock, $f = N_A/(N_A + N_B)$. The time evolution of the order parameter is given by Cahn−Hilliard−Cook (or time-dependent Ginzburg−Landau) equation[16,17,65−69,72]

$$\frac{\partial \psi}{\partial t} = M\nabla^2\left(\frac{\delta F[\psi]}{\delta \psi}\right) + \eta\xi(\mathbf{r}, t) \quad (1)$$

where M is a phenomenological mobility constant. The dimensionless time is tM/a_0^2, where the lattice cell size a_0 and M are set to 1. The last term in eq 1 is a noise with amplitude η and $\xi(\mathbf{r}, t)$ being a Gaussian random noise, which satisfies the fluctuation−dissipation theorem. The free energy functional is[16,67−69]

$$F[\psi] = \int d\mathbf{r}\left[H(\psi) + \frac{D}{2}\left|\nabla\psi\right|^2\right] + \frac{B}{2}\int d\mathbf{r}\int d\mathbf{r}' G(\mathbf{r} - \mathbf{r}')\psi(\mathbf{r})\psi(\mathbf{r}') \quad (2)$$

where

$$H(\psi) = \left[-\frac{\tau}{2} + \frac{A}{2}(1 - 2f)^2\right]\psi^2 + \frac{v}{3}(1 - 2f)\psi^3 + \frac{u}{4}\psi^4 \quad (3)$$

with τ, A, v, u, D, and B being phenomenological parameters, and $G(\mathbf{r} - \mathbf{r}')$ is the Laplace equation Green function.[69] All of these parameters can be related to molecular characteristics. According to Ohta and Kawasaki,[70] $\tau' = -\tau + A(1 - 2f)^2$, D, and B can be expressed in terms of degree of polymerization N, the segment length b, and the Flory−Huggins parameter χ (which is inversely proportional to temperature), as

$$\tau' = -\frac{1}{2N}\left(N\chi - \frac{s(f)}{4f^2(1 - f)^2}\right)$$
$$D = \frac{b^2}{48f(1 - f)}$$
$$B = \frac{9}{4N^2b^2f^2(1 - f)^2} \quad (4)$$

where $s(f)$ is an empirical fitting function of the order of 1 (*e.g.*, $s(0.5) = 0.9$, $s(0.3) = 1.0$).[65,70] In simulation, we use dimensionless parameters $\tilde{D} = D/a_0^2$ and $\tilde{B} = Ba_0^2$ (for simplicity, we keep notations D and B instead of $\tilde{D}$ and $\tilde{B}$). The parameters u and v do not allow for a compact representation and can be computed by evaluating the appropriate vertex function given by Leibler.[71] These are very complex functions that can be only approximately replaced by a constant. We believe that the phenomenology we are studying is quite general, and hence, we allow the freedom of choosing the parameters in eq 2 as phenomenological constants. For the boundary condition, we choose the most simple model in which the preference of copolymer blocks to both surfaces is described by Dirichlet boundary conditions $\psi(R_i) = \psi_i$ ($i = 1, 2$). For instance, for a symmetric lamellae $f = 0.5$, the order parameter in eq 1 becomes $\psi = \phi_A - \phi_B$. Therefore, varying ψ_i, we effectively model the affinity of the surfaces toward one or another block copolymer component. A high performance parallel CDS code was used in our simulations.[72]

Experimental. ***Chemicals and Substrates.*** Aqueous dispersions of silica particles with a diameter of 0.52 μm were obtained from Microparticles GmbH. As substrates, p-type silicon wafers from CrysTech as well as mica sheets from Plano were used. Toluene and chloroform were purchased from VWR, 2,6-di-*tert*-butyl-*p*-cresole (BHT) and osmium tetroxide from Sigma Aldrich, sodium chloride from Grüssing (purity for all 99%), hydrogen peroxide (30%) from Riedel-de Häen, and sulfuric acid (95%) from Fisher Scientic.

Poly(diallyldimethylammonium chloride) (PDADMAC) (20% aqueous solution, molecular weight 100−200 kg/mol, Aldrich) was diluted to a concentration of 1 mg/mL in 0.5 M sodium chloride solution.

A poly(styrene$^{13.7}$-*b*-butadiene$^{33.6}$) block copolymer with a total molecular weight of 47.3 kg/mol and polydispersity index of 1.03 was purchased from Polymer Source Inc. The polymer forms polystyrene cylinders in a polybutadiene matrix. In order to obtain films of 40 nm thickness, the polymer was dissolved in toluene at a concentration of (1 wt %) with 0.03 wt % of BHT in relation to the weight of the polymer. The domain spacing of the BCP is about 32 nm.

Sample Preparation. Silicon substrates were cut in pieces of 1 cm^2 in size and cleaned in toluene for 1 day. Prior to use, the wafer surface was cleaned by snow jet and treated with air plasma for 1 min at 0.2 mbar. When mica was used as a substrate, the top layer of the silicate was cleaved off.

For random distribution of the silica particles, the substrates were coated with a PDADMAC monolayer; 100 μL of PDADMAC solution was put on the wafers for 15 min, subsequently rinsed with water, and dried. The initial dispersions of silica particles were diluted with water to $c = 0.5$ wt % and treated with ultrasound for 10 min; 50 μL of diluted particle dispersion was distributed on the substrates by spin coating at 2000 rpm for 1 min. In order to fix the particles on the substrate, the samples were sintered at 1100 °C for 30 min. Prior to further use, the particle decorated substrates were cleaned with piranha solution (hydrogen peroxide and sulfuric acid in a ratio of 1:3) for 10 min, washed with water, and dried. A part of the substrates was coated with a 16 nm thick carbon film by vapor deposition.

A simple spin coating of the polymer film directly onto the particle decorated substrates led to dewetting of the polymer film on top of the spheres due to thickness variations. In order to ensure a homogeneous thickness over the whole particle, the polymer films were first prepared on mica by spin coating (50 μL, 2000 rpm, 1 min). By slowly dipping the sample into water, the polymer film can be floated from the mica, caught with a particle decorated substrate, and dried.

To obtain the equilibrium state of the polymer morphology, the films were annealed at high temperature or in chloroform solvent vapor. The annealing at elevated temperature was carried out for 18 h under vacuum (20 mbar) at 120 °C. Removing the samples from the oven freezes the structures. The annealing in solvent vapor was performed in a homemade glass chamber, which was sealed to ensure a solvent saturated atmosphere. Subsequently, the samples were inserted and annealed between 15 and 60 min. To freeze the polymer morphology, the samples were transferred to a nitrogen-flushed chamber.

The samples were characterized by scanning force microscopy (SFM) in tapping mode with a Nanoscope IIIm Metrology and Dimension 3100 Controller. Microcantilevers DMCL-AC16OTS from Olympus with a resonance frequency of 301.5−343.0 Hz and a spring constant of 43.0−63.8 N/m were used.

Acknowledgment. M.P. was supported by Accelrys Ltd. *via* EPSRC CASE research studentship. All simulations were performed on SGI Altix 3700 supercomputer at UCLan High Performance Computing Facilities. A.B. and S.H. acknowledge support from the Lichtenberg-Programm of the VolkswagenStiftung.

REFERENCES AND NOTES

1. *Nanostructured Soft Matter, Experiment, Theory, Simulation and Perspectives*; Zvelindovsky, A. V., Ed.; Springer: Dordrecht, The Netherlands, 2007.
2. Hamley, I. W. Nanostructures Fabrication Using Block Copolymers. *Nanotechnology* **2003**, *14*, R39–R54.
3. Park, C.; Yoon, J.; Thomas, E. L. Enabling Nanotechnology with Self Assembled Block Copolymer Pattern. *Polymer* **2003**, *44*, 6725–6760.
4. Urbas, A.; Sharp, R.; Fink, Y.; Thomas, E. L.; Xenidou, M.; Fetters, L. J. Tunable Block Copolymer/Homopolymer Photonic Crystals. *Adv. Mater.* **2000**, *12*, 812–814.
5. Broz, P.; Driamov, S.; Ziegler, J.; Ben-Haim, N.; Marsch, S.; Meier, W.; Hunziker, P. Toward Intelligent Nanosize Bioreactors: A pH-Switchable, Channel-Equipped, Functional Polymer Nanocontainer. *Nano Lett.* **2006**, *6*, 2349–2353.
6. Chen, W.-Q.; Wei, H.; Li, S.-L.; Feng, J.; Nie, J.; Zhang, X.-Z.; Zhuo, R.-X. Fabrication of Star-Shaped, Thermo-Sensitive Poly-(*N*-isopropylacrylamide)-cholic Acid-poly(ε-

caprolactone) Copolymers and Their Self-Assembled Micelles as Drug Carriers. *Polymer* **2008**, *49*, 3965–3972.
7. Sakurai, S. Progress in Control of Microdomain Orientation in Block Copolymers Efficiencies of Various External Fields. *Polymer* **2008**, *49*, 2781–2796.
8. Sivaniah, E.; Hayashi, Y.; Matsubara, S.; Kiyono, S.; Hashimoto, T.; Fukunaga, K.; Kramer, E. J.; Mates, T. Symmetric Diblock Copolymer Thin Films on Rough Substrates. Kinetics and Structure Formation in Pure Diblock Copolymer Thin Films. *Macromolecules* **2005**, *38*, 1837–1849.
9. Fukunaga, K.; Hashimoto, T.; Elbs, H.; Krausch, G. Self-Assembly of a Lamellar ABC Triblock Terpolymer Thin Film. Effect of Substrates. *Macromolecules* **2003**, *36*, 2852–2861.
10. Olszowka, V.; Tsarkova, L.; Böker, A. 3 Dimensional Control over Lamellae Orientation and Order in Thick Block Copolymer Films. *Soft Matter* **2009**, *5*, 812–819.
11. Knoll, A.; Tsarkova, L.; Krausch, G. Nanoscaling of Microdomain Spacing in Thin Films of Cylinder-Forming Block Copolymers. *Nano Lett.* **2007**, *7*, 843–846.
12. Fasolka, M. J.; Mayes, A. M. Block Copolymer Thin Films: Physics and Applications. *Annu. Rev. Mater. Res.* **2001**, *31*, 323–355.
13. van Zoelen, W.; ten Brinke, G. Thin Films of Complexed Block Copolymers. *Soft Matter* **2009**, *5*, 1568–1582.
14. Xu, T.; Craig, J. H.; Russell, T. P. Interfacial Energy Effects on the Electric Field Alignment of Symmetric Diblock Copolymers. *Macromolecules* **2003**, *36*, 6178–6182.
15. Böker, A.; Schmidt, K.; Knoll, A.; Zettl, H.; Hansel, H.; Urban, V.; Abetz, V.; Krausch, G. The Influence of Incompatibility and Dielectric Contrast on the Electric Field-Induced Orientation of Lamellar Block Copolymers. *Polymer* **2006**, *47*, 849–857.
16. Pinna, M.; Zvelindovsky, A. V.; Todd, S.; Goldbeck-Wood, G. Cubic Phases of Block Copolymers under Shear and Electric Fields by Cell Dynamics Simulation. I. Spherical Phase. *J. Chem. Phys.* **2006**, *125*, 154905.
17. Pinna, M.; Zvelindovsky, A. V. Kinetic Pathways of Gyroid-to-Cylinder Transitions in Diblock Copolymers under External Fields: Cell Dynamics Simulation. *Soft Matter* **2008**, *4*, 316–327.
18. Matsen, M. W. Undulation Instability in Block-Copolymer Lamellae Subjected to a Perpendicular Electric Field. *Soft Matter* **2006**, *2*, 1048–1056.
19. Schmidt, K.; Böker, A.; Zettl, H.; Schubert, F.; Hänsel, H.; Fischer, F.; Weiss, T. M.; Abetz, V.; Zvelindovsky, A. V.; Sevink, G. J. A.; Krausch, G. Influence of Initial Order on the Microscopic Mechanism of Electric Field Induced Alignment of Block Copolymer Microdomains. *Langmuir* **2005**, *21*, 11974–11980.
20. Böker, A.; Elbs, H.; Hänsel, H.; Knoll, A.; Ludwigs, S.; Zettl, H.; Zvelindovsky, A. V.; Sevink, G. J. A.; Urban, V.; Abetz, V.; Müller, A. H. E.; Krausch, G. Electric Field Induced Alignment of Concentrated Block Copolymer Solutions. *Macromolecules* **2003**, *36*, 8078–8087.
21. Hong, Y.-R.; Admson, D. H.; Chainkin, P. M.; Register, R. A. Shear-Induced Sphere-to-Cylinder Transition in Diblock Copolymer Thin Films. *Soft Matter* **2009**, *5*, 1687–1691.
22. Kellogg, G. J.; Walton, D. G.; Mayes, A. M.; Lambooy, P.; Russell, T. P.; Gallagher, P. D.; Satija, S. K. Observed Surface Energy Effects in Confined Diblock Copolymers. *Phys. Rev. Lett.* **1996**, *76*, 2503–2506.
23. Huang, E.; Russell, T. P.; Harrison, c.; Chaikin, P. M.; Register, R. A.; Hawker, C. J.; Mays, J. Using Surface Active Random Copolymers To Control the Domain Orientation in Diblock Copolymer Thin Films. *Macromolecules* **1998**, *31*, 7641–7650.
24. Wang, Q.; Yan, Q.; Nealey, P. F.; de Pablo, J. J. Monte Carlo Simulations of Diblock Copolymer Thin Films Confined between Chemically Heterogeneous Hard Surfaces. *Macromolecules* **2000**, *33*, 4512–4525.
25. Matsen, M. W. Thin Films of Block Copolymer. *J. Chem. Phys.* **1997**, *106*, 7781–7791.
26. Horvat, A.; Lyakhova, K. S.; Sevink, G. J. A.; Zvelindovsky, A. V.; Magerle, R. Phase Behavior in Thin Films of Cylinder-Forming ABA Block Copolymers: Mesoscale Modeling. *J. Chem. Phys.* **2004**, *120*, 1117–1126.
27. Lyakhova, K. S.; Sevink, G. J. A.; Zvelindovsky, A. V.; Horvat, A.; Magerle, R. Role of Dissimilar Interfaces in Thin Films of Cylinder-Forming Block Copolymers. *J. Chem. Phys.* **2004**, *120*, 1127–1137.
28. Horvat, A.; Sevink, G. J. A.; Zvelindovsky, A. V.; Krekhov, A.; Tsarkova, L. Specific Features of Defect Structure and Dynamics in the Cylinder Phase of Block Copolymers. *ACS Nano* **2008**, *2*, 1143–1152.
29. Knoll, A.; Lyakhova, K. S.; Horvat, A.; Krausch, G.; Sevink, G. J. A.; Zvelindovsky, A. V.; Magerle, R. Direct Imaging and Mesoscale Modelling of Phase Transitions in a Nanostructured Fluid. *Nat. Mater.* **2004**, *3*, 887–890.
30. Knoll, A.; Horvat, A.; Lyakhova, K. S.; Krausch, G.; Sevink, G. J. A.; Zvelindovsky, A. V.; Magerle, R. Phase Behavior in Thin Films of Cylinder-Forming Block Copolymers. *Phys. Rev. Lett.* **2002**, *89*, 035501.
31. Knoll, A.; Magerle, R.; Kraush, G. Phase Behavior in Thin Films of Cylinder-Forming ABA Block Copolymers: Experiments. *J. Chem. Phys.* **2004**, *120*, 1105–1116.
32. Xiang, H.; Shin, K.; Kim, T.; Moon, S. I.; McCarthy, T. J.; Russell, T. P. Block Copolymers under Cylindrical Confinement. *Macromolecules* **2004**, *37*, 5660–5664.
33. Shin, K.; Xiang, H.; Moon, S. I.; Kim, T.; McCarthy, T. J.; Russel, T. P. Curving and Frustrating Flatland. *Science* **2004**, *306*, 76.
34. Wu, Y.; Cheng, G.; Katsov, K.; Sides, S. W.; Wang, J.; Tang, J.; Fredrickson, G. H.; Moskovits, M.; Stucky, G. D. Composite Mesostructures by Nano-Confinement. *Nat. Mater.* **2004**, *3*, 816–822.
35. Xiang, H.; Shin, K.; Kim, T.; Moon, S.; McCarthy, T. J.; Russell, T. P. The Influence of Confinement and Curvature on the Morphology of Block Copolymers. *J. Polym. Sci., Part B: Polym. Phys.* **2005**, *43*, 3377–3383.
36. He, X.; Song, M.; Liang, H.; Pan, C. Self-Assembly of the Symmetric Diblock Copolymer in a Confined State: Monte Carlo Simulation. *J. Chem. Phys.* **2001**, *114*, 10510–10513.
37. Sevink, G. J. A.; Zvelindovsky, A. V.; Fraaije, J. G. E. M. Morphology of Symmetric Block Copolymer in a Cylindrical Pore. *J. Chem. Phys.* **2001**, *115*, 8226–8230.
38. Li, W.; Wickham, R. A.; Garbary, R. A. Phase Diagram for a Diblock Copolymer Melt under Cylindrical Confinement. *Macromolecules* **2006**, *39*, 806–811.
39. Chen, P.; He, X.; Liang, H. Effect of Surface Field on the Morphology of a Symmetric Diblock Copolymer under Cylindrical Confinement. *J. Chem. Phys.* **2006**, *124*, 104906.
40. Yu, B.; Sun, P.; Chen, T.; Jin, Q.; Ding, D.; Li, B.; Shi, A.-C. Confinement-Induced Novel Morphologies of Block Copolymers. *Phys. Rev. Lett.* **2006**, *96*, 138306.
41. Feng, J.; Liu, H.; Hu, Y. Mesophase Separation of Diblock Copolymer Confined in a Cylindrical Tube Studied by Dissipative Particle Dynamics. *Macromol. Theory Simul.* **2006**, *15*, 674–685.
42. Feng, J.; Ruckenstein, E. Morphologies of AB Diblock Copolymer Melts Confined in Nanocylindrical Tubes. *Macromolecules* **2006**, *39*, 4899–4906.
43. Xiao, X.; Huang, Y.; Liu, H.; Hu, Y. Morphology Transition of Block Copolymers under Curved Confinement. *Macromol. Theory Simul.* **2007**, *16*, 732–741.
44. Sevink, G. J. A.; Zvelindovsky, A. V. Block Copolymers Confined in a Nanopore: Pathfinding in a Curving and Frustrating Flatland. *J. Chem. Phys.* **2008**, *128*, 084901.
45. Wang, Z.; Li, B.; Jin, Q; Ding, D.; Shi, A.-C. Simulated Annealing Study of Self-Assembly of Symmetric ABA Triblock Copolymers Confined in Cylindrical Nanopores. *Macromol. Theory Simul.* **2008**, *17*, 86–102.
46. Wang, Z.; Li, B.; Jin, Q; Ding, D.; Shi, A.-C. Self-Assembly of Cylinder-Forming ABA Triblock Copolymers under Cylindrical Confinement. *Macromol. Theory Simul.* **2008**, *17*, 301–312.
47. Pinna, M.; Guo, X.; Zvelindovsky, A. V. Diblock Copolymers in a Cylindrical Pore. *J. Chem. Phys.* **2009**, *131*, 214902.

48. Sachdev, S.; Nelson, D. R. Crystallyne and Fluid Order on a Random Topography. *J. Phys. C* **1984**, *17*, 5473–5489.
49. Kamien, R. D.; Nelson, D. R.; Santangelo, C. D.; Vitelli, V. Extrinsic Curvature, Geometric Optics, and Lamellar Order on Curved Substrates. *Phys. Rev. E* **2009**, *80*, 051703.
50. Jackson, A. M.; Myerson, J. W.; Stellacci, F. Spontaneous Assembly of Subnanometreordered Domains in the Ligand Shell of Monolayer-Protected Nanoparticles. *Nat. Mater.* **2004**, *3*, 330–336.
51. Yabu, H.; Higuchi, T.; Ljiro, K.; Shimomura, M. Spontaneous Formation of Polymer Nanoparticles by Good-Solvent Evaporation as a Nonequilibrium Process. *Chaos* **2005**, *15*, 047505.
52. Yabu, H.; Higuchi, T.; Shimomura, M. Unique Phase-Separation Structures of Block-Copolymer Nanoparticles. *Adv. Mater.* **2005**, *17*, 2062–2065.
53. Kim, H.; Daniels, E. S.; Li, S.; Mokkapati, V. K.; Kardos, K. Polymer Encapsulation of Yttrium Oxysulfide Phosphorescent Particles via Miniemulsion Polymerization. *J. Polym. Sci., Part A: Polym. Chem.* **2007**, *45*, 1038–1054.
54. Such, G. K.; Tjipto, E.; Postma, A.; Johnston, A. P. R.; Caruso, F. Ultrathin, Responsive Polymer Click Capsules. *Nano Lett.* **2007**, *7*, 1706–1710.
55. Higuchi, T.; Yabu, H.; Shimomura, M. Differences of Internal Structures between Amphiphilic and Hydrophobic Block-Copolymer Nanoparticles. *J. Nanosci. Nanotechnol.* **2007**, *7*, 1–3.
56. Tajima, A.; Higuchi, T.; Yabu, H.; Shimomura, M. Hemispherical Polymer Nano-particles of Polyisoprene-Poly(methyl methacrylate) Blend with Core−Shell Structure. *Colloids and Surfaces A: Physicochem. Eng. Aspects* **2007**, *16*, 332–334.
57. Rider, D. A.; Chen, J. I. L.; Eloi, J.-C.; Arsenault, A. C.; Russell, T. P.; Ozin, G. A.; Manners, I. Controlling the Morphologies of Organometallic Block Copolymers in the 3-Dimensional Spatial Confinement of Colloidal and Inverse Colloidal Crystals. *Macromolecules* **2008**, *41*, 2250–2259.
58. Higuchi, T.; Tajima, A.; Yabu, H.; Shimomura, M. Spontaneous Formation of Polymer Nanoparticles with Inner Micro-Phase Separation Structures. *Soft Matter* **2008**, *4*, 1302–1305.
59. Tang, P.; Qiu, F.; Zhang, H.; Yang, Y. Phase Separation Patterns for Diblock Copolymers on Spherical Surfaces: A Finite Volume Method. *Phys. Rev. E* **2005**, *72*, 016710.
60. Chantawansri, T. L.; Bosse, A. W.; Hexemer, A; Ceniceros, H. D.; Garcia-Cervera, C. J.; Kramer, E. J.; Fredrickson, G. H. Self-Consistent Field Theory Simulations of Block Copolymer Assembly on a Sphere. *Phys. Rev. E* **2007**, *75*, 031802.
61. Sevink, G. J. A.; Zvelindovsky, A. V. Self-Assembly of Complex Vesicles. *Macromolecules* **2005**, *38*, 7502–7513.
62. Uneyama, T. Density Functional Simulation of Spontaneous Formation of Vesicle in Block Copolymer Solutions. *J. Chem. Phys.* **2007**, *126*, 114902.
63. Fraaije, J. G. E. M.; Sevink, G. J. A. Model for Pattern Formation in Polymer Surfactant Nanodroplets. *Macromolecules* **2003**, *36*, 7891–7893.
64. Yu, B.; Li, B.; Jin, Q.; Ding, D.; Shi, A.-C. Self-Assembly of Symmetric Diblock Copolymers Confined in Spherical Nanopores. *Macromolecules* **2007**, *40*, 9133–9142.
65. Pinna, M.; Guo, X.; Zvelindovsky, A. V. Block Copolymer Nanoshells. *Polymer* **2008**, *49*, 2797–2800.
66. Oono, Y; Puri, S. Study of Phase-Separation Dynamics by Use of Cell Dynamical Systems. I. Modeling. *Phys. Rev. A* **1988**, *38*, 434–453.
67. Bahiana, M.; Oono, Y. Cell Dynamical System Approach to Block Copolymers. *Phys. Rev. A* **1990**, *41*, 6763–6771.
68. Qi, S.; Wang, Z.-G. Kinetics of Phase Transitions in Weakly Segregated Block Copolymers: Pseudostable and Transient States. *Phys. Rev. E* **1997**, *55*, 1682–1697.
69. Ren, S. R.; Hamley, I. W. Cell Dynamics Simulations of Microphase Separation in Block Copolymers. *Macromolecules* **2001**, *34*, 116–126.
70. Ohta, T.; Kawasaki, K. Equilibrium Morphology of Block Copolymer Melts. *Macromolecules* **1986**, *19*, 2621–2632.
71. Leibler, L. Theory of Microphase Separation in Block Copolymers. *Macromolecules* **1980**, *13*, 1602–1617.
72. Guo, X.; Pinna, M.; Zvelindovsky, A. V. Parallel Algorithm for Cell Dynamics Simulation of Block Copolymers. *Macromol. Theory Simul.* **2007**, *16*, 779–784.
73. Rehse, S.; Mecke, K.; Magerle, R. Characterization of the Dynamics of Block Copolymer Microdomains with Local Morphological Measures. *Phys. Rev. E* **2008**, *77*, 051805.
74. Mecke, K. R. Morphological Characterization of Patterns in Reaction-Diffusion Systems. *Phys. Rev. E* **1996**, *53*, 4794–4800.